Dynamical Maps of the Inner Asteroid Belt

Tatiana A. Michtchenko[1], **Daniela Lazzaro**[2], **Jorge M. Carvano**[2], **and Sylvio Ferraz-Mello**[1]

[1]Instituto de Astronomia, Geofísica e Ciências Atmosféricas, USP, Rua do Matão 1226, 05508-900 São Paulo, Brazil
email: `tatiana@astro.iag.usp.br`

[2]Observatório Nacional, R. Gal. José Cristino 77, 20921-400, Rio de Janeiro, Brazil

Abstract. We construct the dynamic portrait of the inner asteroidal belt using the information about the distribution of the test particles, which were initially placed on a perfectly rectangular grid of initial conditions, after 4.2 Myr of gravitational interactions with the Sun and five planets, from Mars to Neptune. Using the Spectral Analysis Method introduced by Michtchenko *et al.* (2002), we illustrate the asteroidal behaviour on the dynamical maps. We superpose over the maps the information on the proper elements and proper frequencies of the real objects, extracted from the database *AstDyS* (Milani & Knežević 1994; Knežević & Milani 2003). The comparison of the maps with the distribution of the real objects allows us to detect possible dynamical mechanisms acting in the domain under study: these mechanisms are related to mean-motion and secular resonances. Their long-lasting action, overlaying with the Yarkovsky effect, may explain many observed features of the distribution of the asteroids.

Keywords. minor planets; asteroids, dynamics

1. Introduction

It is nowadays accepted that many features of the asteroid distribution may be explained by long-lasting actions of dynamical mechanisms, present in the inner main belt. With purpose to identify these mechanisms, we elaborate a global dynamic picture of the inner part of the main belt, using the Spectral Analysis Method introduced by Michtchenko *et al.* (2002). The main idea of the method consists of using the information about the distribution of the test particles, which were initially placed over a perfectly rectangular grid of initial conditions, after 4.2 Myr of gravitational interactions with the Sun and five planets, from Mars to Neptune.

The final distribution of the fictitious particles will reflect the peculiarities of dynamical interactions between asteroids and the planets in the region under study. Particulary, the test particles will preserve (at least, during the time span covered by integrations) some invariable quantities of motion (e.g. proper elements), if they belong to the domains of quasi-regular motion. In contrast, these quantities will exhibit variations in the domains of dynamical instabilities, which can result even in the escape of the objects from the studied region. Therefore, the test particles can form agglomerations or, on the contrary, some voids in the specific regions of the phase space, due to the action of mean-motion and secular resonances, in such a way indicating the location of these features.

2. Dynamical maps on the representative planes

At the present, there are around 200,000 numbered objects in Bowell's catalogue of asteroid orbital elements (Bowell *et al.* 1994). About 60,000 objects are found in the

range of proper semimajor axis between 2.1 AU and 2.5 AU. This region of the main belt is often referred to as the inner part.

To construct the dynamical portrait of the inner belt in the three-dimensional elements space, we introduce so-called 'representative planes' (Milani & Knežević 1992): the sample of the objects is separated in different eccentricity intervals and each one is presented on the (a, I)–plane of the semimajor axis and inclination. We have chosen arbitrarily four eccentricity intervals; inside each interval we identified one known dynamical family and associated the name of this family to the interval. We also used the values of the osculating eccentricity and angular elements of the main object of the family as the input of numerical integrations, to construct the dynamical maps.

The first interval is characterized by very low eccentricities, less than 0.075. There are neither known families nor clusters, so we select one large object from this interval, 230 Athamantis with magnitude 7.3, and associate it to this interval. The next interval
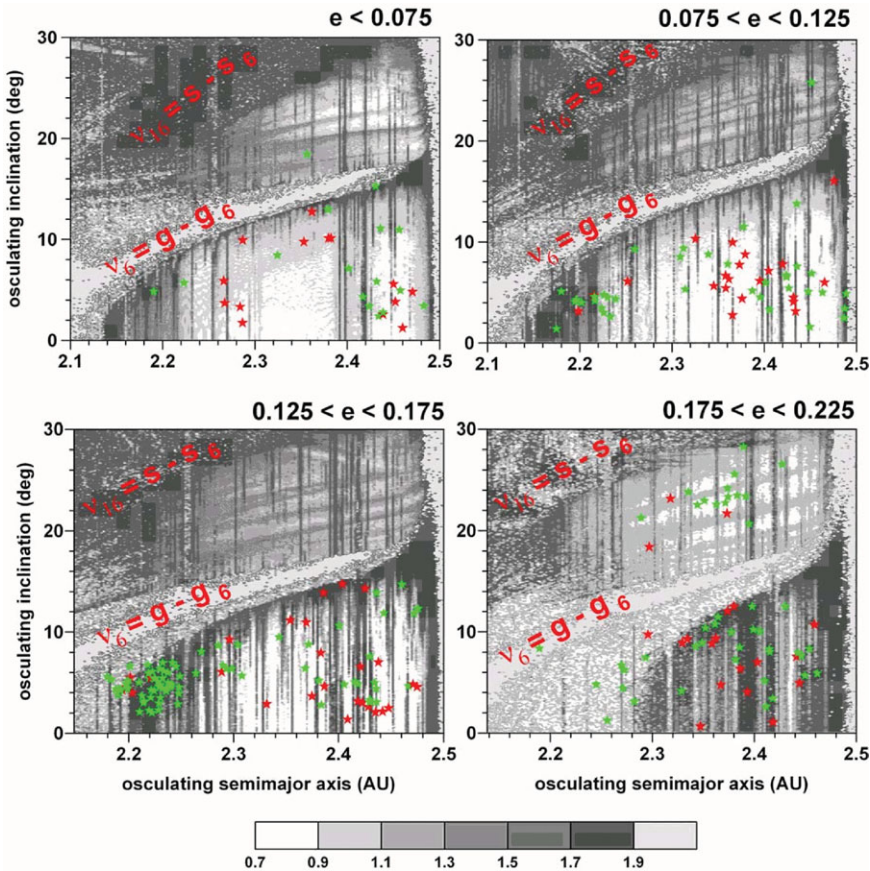
Figure 1. Dynamical maps around: 230 Athamantis (left-top panel), 4 Vesta (right-top panel), 298 Baptistina (left-bottom panel) and 163 Erigone (right-bottom panel) on the (a, I)–planes of the osculating semimajor axis and inclination. The gray color levels correlate the stochasticity of motion with the spectral number N, in logarithmic scale: lighter regions corresponds to regular motion, while darker tones indicate increasingly chaotic motion. The hatched regions correspond to initial conditions that lead to escape of objects in less than 4.2 Myr. The real objects from the corresponding eccentricity interval are superposed on each graph: red stars are objects with magnitudes less than 10, while green stars are objects with magnitudes in the range from 10 to 12.

is centered around 4 Vesta and covers low-to-moderate eccentricities within the range $0.075 \leqslant e < 0.125$. Finally, the next two intervals are associated to 298 Baptistina and 163 Erigone and cover the moderate ($0.125 \leqslant e < 0.175$) and high ($0.175 \leqslant e < 0.225$) eccentricities, respectively.

60300 massless particles were chosen in each eccentricity interval: their initial semi-major axes and inclinations were distributed over a rectangular 201×300 grid, covering the representative plane. Each particle has been integrated over 4.2 Myr, accounting for planetary perturbations from Mars to Neptune. During the integration, a low pass-band digital filter has been applied to remove the short period oscillations of the order of orbital periods.

The output series of filtered elements for each test orbit have been Fourier analyzed, in order to identify the relevant peaks in their Fourier spectra. The number of the relevant peaks in the semimajor axis variation, known as a 'spectral number N', was used to characterize the chaoticity of the orbit: for regular orbits with small values of N, a few well defined lines appear in the spectra, while for chaotic orbits the number of peaks (consequently, N) is huge. This information has been translated to a gray scale code and plotted on the (a_{osc}, I_{osc})–planes of the osculating semimajor axis and inclination.

Figure 1 shows the dynamical maps of the inner main belt plotted on planes corresponding to different eccentricity intervals. Since the variation of the asteroidal semimajor axis is strongly affected by mean-motion resonances, its time evolution was chosen as a basis for calculation of N. The calculated values of N, in the range from 1 to 80, were coded by a gray level scale that varied logarithmically from white ($\log N = 0$) to black ($\log N = 1.9$). Large values of N indicate the onset of chaos, while lighter regions on the dynamical maps correspond to regular motion, and darker tones indicate increasingly chaotic motion. The domains, where the test particles escape from the region within the time-interval of integration (~ 4.2 Myr), are hatched.

On the dynamical maps in Fig. 1 we superpose proper elements of some real objects from the corresponding eccentricity range. Only large objects are shown, those with absolute magnitudes lower than 10 (red stars) and between 10 and 12 (green stars). It is worth emphasizing that the dynamical map constructed over a grid of osculating orbital elements cannot be directly compared to the proper elements of the asteroids; thus, Figure 1 provide only an estimation of the dynamical distribution of real objects.

The dominant effects on the asteroidal motion are produced by the strong secular resonances, ν_6 and ν_{16}. The ν_6 secular resonance occurs in the regions where the precessional rate of the asteroid's longitude of perihelion equals the precessional rate of Saturn's perihelion. The ν_6 resonance is responsible for large-scale instabilities followed by rapid escape of the test particles inside diagonal bands crossing all maps from the lower-left to the upper-right corners in Fig. 1. The bulk of real objects is located below this band, forming the low inclination population.

The ν_{16} secular resonance occurs in the regions where the precessional rate of the asteroid's longitude of node equals the precessional rate of Saturn's node. The ν_{16} SR produces the large domains of chaotic motion in the high inclination zones and forms a natural upper boundary of the asteroidal population in the inner belt. High inclination domains of quasi-regular motion can be observed between the ν_6 and ν_{16} resonances, on each panel in Fig. 1. The curious feature is the absence of high inclined asteroids (at least, with $mag < 12$) at low and moderate eccentricities. This population is significant only at $e > 0.18$. The motion of the objects in this region is highly nonharmonic (later we will associate this property to the action of nonlinear secular resonances). Despite this fact, the 25 Phocaea, 5247 Krylov and 1660 Wood groups are found inside the high inclination zone.

A relevant feature clearly visible in Fig. 1, is the occurrence of several vertical stripes of chaotic motion, which are associated with two- and three-body mean-motion resonances with the planets from Mars to Uranus. The dominating mean-motion resonance is the 3J/1A mean-motion resonance with Jupiter, whose region is strongly chaotic, with rapid escapes of the test particles (the right border of all graphs). Thus, the devastating effects of the 3J/1A mean-motion resonance, together with ν_{16} SR, create the physical boundaries of the inner belt, while ν_6 SR delimits the domains of the low inclination orbits.

Apart the 3J/1A resonance, mean-motion resonances in the inner belt are weak: this is due to the large distance from the Jupiter–Saturn system and the small mass of Mars. Many of these resonances cut through the asteroid families and we may expect several family members to have involved in the resonances. Among the mostly relevant ones, there are 7J/2A MMR with Jupiter and 1M/2A MMR with Mars. There are also several three-body mean-motion resonances of low order, such as the $4J : -1S : -1A$, $4J : -2S : -1A$, and $5J : -4S : -1A$ resonances, where the letters J, S, A denote Jupiter, Saturn and an asteroid, respectively.

It is known that the density and the strength of the mean-motion resonances increase with increasing eccentricities; moreover, at high eccentricities, many of them may overlap creating the domains of unstable motion. The low inclination region on the bottom-right panel in Fig. 1 showing high indices of stochasticity, seems to confirm this assumption. The surprising fact is that this region is significantly populated by large objects. Moreover, this population strongly contrasts with the population on the nearly circular orbits (see top-left panel in the same figure), which does not undergo the action of the overlapping mean-motion resonances, but presents low density of large objects.

References

Bowell, E., Muinonen, K., & Wasserman, L. H. 1994, in: A. Milani, M. di Martino & A. Cellino (eds.), *Asteroid, Comets and Meteorids III*, (Dordrecht: Kluwer), p. 477

Michtchenko, T., Lazzaro, D., Ferraz-Mello, S., & Roig, F. 2002, *Icarus*, 158, 343

Milani, A. & Knežević, Z. 1992, *Icarus*, 98, 211

Milani, A. & Knežević, Z. 1992, *Icarus*, 107, 219